A Modular Biological Neural Network-Based Neuro-Robotic System via Local Chemical Stimulation and Calcium Imaging

Zhe Chen, Xie Chen, Shingo Shimoda, Qiang Huang, Qing Shi, Toshio Fukuda, and Tao Sun

***Abstract*—Embodying in vitro biological neural networks (BNNs) with robots to explore the rise of intelligence in these simpler models and to endow robots with biological intelligence has been attracting increasing attention in the fields of neuroscience and robotics. However, current research suffers from unstable sensory-motor mapping due to the random wiring of neurons seeded on multi-electrode arrays (MEAs). Therefore, here we propose a modular BNN (mBNN)-based neuro-robotic system via local chemical stimulation and calcium recording. In this system, reliable evoked sensory-motor mapping (success rate $>$ 89%) from the sensory to the motor area in the mBNN was demonstrated. It is achieved in the mBNNs by combining global chemical modulation (for suppressing spontaneous signal transmission) and local chemical stimulation (for inducing the evoked signal transmission). The neural signals of the motor area of the BNN are recorded by calcium imaging, analyzed, and decoded to control the motion state of the mobile robot in real-time. The sensory signals of the robot are encoded and transmitted to the sensory area of the BNN, closing the loop. This system presents a platform to investigate how information is processed and transmitted in mBNNs, and also to examine the influence of local and global chemical modulation on within-network signal transmission.**

***Index Terms*—Neurorobotics, cyborgs, biological neural networks, neuro-robotic systems.**

Manuscript received 8 February 2023; accepted 19 July 2023. Date of publication 2 August 2023; date of current version 9 August 2023. This letter was recommended for publication by Associate Editor T. Taniguchi and Editor T. Ogata upon evaluation of the reviewers' comments. This work was supported by the National Natural Science Foundation of China under Grants 62173043, 62022014, and 62088101. *(Corresponding authors: Tao Sun.)*

Zhe Chen is with the School of Medical Technology, Beijing Institute of Technology, Beijing 100081, China, also with the Beijing Advanced Innovation Center for Intelligent Robots and Systems, Beijing Institute of Technology, Beijing 100081, China, and also with the Key Laboratory of Biomimetic Robots and Systems (Beijing Institute of Technology), Ministry of Education, Beijing 100081, China (e-mail: zhechen95@bit.edu.cn).

Xie Chen, Qiang Huang, Qing Shi, Toshio Fukuda, and Tao Sun are with the Beijing Advanced Innovation Center for Intelligent Robots and Systems, Beijing Institute of Technology, Beijing 100081, China, and also with the Key Laboratory of Biomimetic Robots and Systems (Beijing Institute of Technology), Ministry of Education, Beijing 100081, China (e-mail: 3120195093@bit.edu.cn; qhuang@bit.edu.cn; shiqing@bit.edu.cn; tofukuda@nifty.com; 6120200193@bit.edu.cn).

Shingo Shimoda is with the RIKEN Center for Brain Science, TOYOTA Collaboration Center, RIKEN, Nagoya 463-0003, Japan (e-mail: shingo.shimoda@riken.jp).

This letter has supplementary downloadable material available at https://doi.org/10.1109/LRA.2023.3301233, provided by the authors.

Digital Object Identifier 10.1109/LRA.2023.3301233

I. Introduction

BIOLOGICAL neural network (BNN)-based neuro-robotic systems feature in vitro BNNs for mapping input (sensory) signals to output (motor) signals, compared with traditional robotic systems. They were recently proposed as a platform to investigate how information is processed and encoded in BNNs in vitro [1]. On one hand, in these systems, primary neurons were dissociated to reconstruct simpler BNNs in vitro, reproducing mini-brains. Many characteristics of in vivo BNNs were rediscovered in the in vitro BNNs, for example, stimulus-dependent synaptic plasticity, supervised learning, input-dependent adaptation, associative memory, logical operation, short-term memory, spatiotemporal memory, unsupervised learning, and homeostatic plasticity, etc. [2], [3], which demonstrates the potential of in vitro BNNs to become as intelligent as their in vivo counterpart (brains). On the other hand, the BNNs (mini-brains) were embodied with robots (bodies) to allow interaction with the environment and further realize biological intelligence in vitro [4], that is, to sense and adapt to the outer world. Therefore, it has attracted increasing attention in both neuroscience and robotics.

Current neuro-robotic systems can be classified into two categories: 1) those that leveraged the BNN for signal transmission, which only transmits simple signals from the sensory (input) area to the motor (output) area [5], [6], [7], [8]; and 2) those that viewed the BNN as a high-dimensional information processer, which maps input signals to complex spatiotemporal patterns of neural activities [9], [10]. For either kind, the key to constructing a reliable neuro-robotic system is the capability to decipher the exact input (sensory) signals according to the recorded signals from output (motor) areas, based on which the robot can respond with appropriate motor outputs to the sensory signals. From this perspective, a biological neural network divided into sensor areas and motor areas (therefore transmitting signals from sensory to motor areas) are more effective for constructing a neuro-robotic system, because the input signals can be more readily and accurately deciphered. For these systems, it is necessary to establish a method of transmitting signals with good reproducibility (reliable sensory-motor mapping). However, for most of the current BNNs-based neuro-robotic systems, the sensory-motor (input-output) mapping is still not stable enough for the robot to perform specific tasks reliably. In particular, Warwick et al. in [5], and Li et al. [8] achieved neurorobotics systems with a

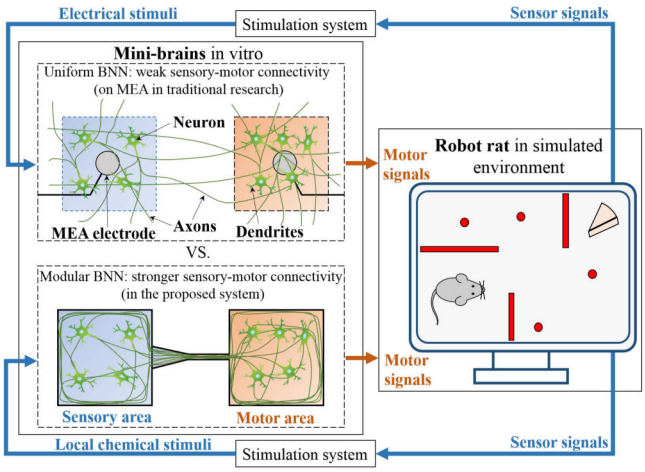

Fig. 1. Stronger sensory-motor connectivity is achieved in the proposed system by setting the BNN to be modularly distributed.

sensory-motor mapping success rate of overall 44.9% (with 67% evoked success rate and 42.1% false-positive rate), and 80%, respectively.

Higher sensory-motor mapping reliability is hard to achieve due to these following problems intrinsic in the mainstream neuro-robotic systems. First, the use of uniformly distributed BNNs formed on multi-electrode arrays (MEAs). Research has shown that signal transmission between neurons is unreliable [11], and neurons in uniformly distributed BNNs wire together randomly. It's difficult to construct reliable sensory-motor mapping in these BNNs. Therefore, some researchers explored the use of modular BNNs to construct neuro-robotic systems for its reliable signal transmission within the modular networks [12], [13], [14]. Second, spontaneous neural activities exist, which may be detected as false-positive mapping (activities detected in the motor area while no stimulation was applied in the sensory area). Moreover, stimulus-evoked signal transmission may be interfered due to spontaneous activity-induced refractoriness [15].

Thus, to achieve more reliable sensory-motor mapping, two improvements are made in the proposed neuro-robotic system. First, the BNN is set to be modularly distributed, comprising two modules (areas): sensory area and motor area. The neurites are confined to grow within or between modules. Therefore, compared with uniformly distributed BNNs, the mBNNs feature a stronger inter-modular connectivity between modules, as shown in Fig. 1. Second, the spontaneous bursts were suppressed. However, suppression would inevitably reduce the network excitability [16], and hence reduce its ability to transmit signals between modules. In this work, we demonstrate that with the spontaneous activities suppressed, reliable evoked sensory-motor mapping (inter-modular signal transmission) can still be achieved with a success rate over 89% by local chemical stimulation.

Therefore, this letter is characterized by a modular BNN-based neuro-robotic system with reliable sensory-motor mapping via local chemical stimulation and calcium imaging in closed-loop and in real-time. In this system, not only reliable evoked sensory-motor mapping is demonstrated, but it's also interconnected with a mobile robot to indicate whether an obstacle is met in front of it, and therefore whether the robot should steer clear of the obstacle or keep moving forward, hence achieving active obstacle avoidance. Specifically, the main contributions of this letter include the following. First, we showed that evoked sensory-motor mapping of burst signals can still be realized in the mBNN by combining whole-field chemical modulation (for suppressing spontaneous activity) and local chemical stimulation, achieving reliable sensory-motor signal transmission. To this end, we custom-designed a cost-effective concentric (double) micropipette to confine chemical stimulation to a desirable spatio-temporal range. Moreover, through a custom-written graphical user interface (GUI), we interconnected the mBNN with a mobile robot (in simulator CoppeliaSim) and demonstrated the sensory-motor mapping is reliable enough to guide the robot to actively avoid obstacles.

II. System Description

The neuro-robotic system consists of an mBNN, a concentric micropipette (for local chemical stimulation), a micromanipulator (for positioning the micropipette), two syringe pumps, an epifluorescence microscope (for calcium imaging), and a PC (for running robot simulator CoppeliaSim, the custom-written GUI, and microscopic software CellSens), as shown in Fig. 2(a). In this system, the GUI receives sensory signals from robot simulator, encodes them into stimuli signals and transmits them to the controller of syringe pumps. At the same time, it also monitors the neural signals of the motor area of the mBNN, decodes them into motor signals, and transmits them back to the robot simulator.

A. mBNN-Based Evoked Intermodular Signal Transmission

The mBNN was fabricated by micro-contact printing and seeding primary neurons. This mBNN comprises two modules (areas), and neurons in the two areas are connected by a nerve bundle. Moreover, under calcium imaging, most neurons in both areas showed spontaneous and simultaneous fluorescence elevation, which was defined as network-wide bursts [17]. This demonstrated the spontaneous inter-modular signal transmission between the two areas. Spontaneous network-wide bursts indicate that the mBNN can transmit signals inter-modularly. However, these spontaneous signals will not only be mistakenly recognized as valid signals (false-positive mapping), but also may interfere with the transmission of valid signals, so it needs to be suppressed. In this work, we first suppress the spontaneous network-wide bursts by elevating $[Mg^{2+}]$ globally, then stimulate the neurons in the sensory area with a neurotransmitter (glutamate) locally.

B. Interconnecting the BNN With a Mobile Robot

Based on local chemical stimulation, we interconnect the mBNN with a mobile robot (in simulator CoppeliaSim), as shown in Fig. 2(b). The interconnection contains two parts: from robot to mBNN and from mBNN to robot. In the former one,

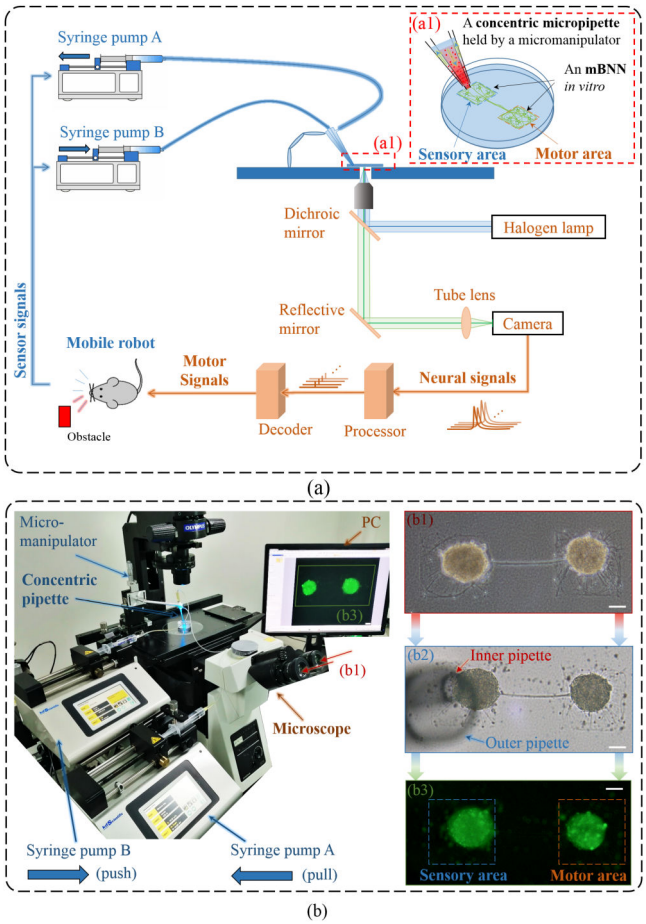

Fig. 2. mBNN-based neuro-robotic system. (a) Schematic of the system. (b) Left: overview of the system; (b1) Phase-contrast micrograph of an mBNN; (b2) Bright-field view of the same mBNN with the concentric pipette positioned above its sensory area; (b3) Epi-fluorescence view. Scale bar: 50 μm.

sensory signals from the robot are transmitted to the custom-made GUI, and encoded to the stimulator (syringe pump), so as to stimulate neurons in the sensory area. Then, area-wide burst signals will be evoked in the sensory area and transmitted to the motor area through the nerve bundle. In the latter part, neurons in the mBNN are monitored by calcium imaging, with the real-time video stream transmitted to the microscopic software cellSens. The GUI selects all the active neurons in the motor area as regions of interest (ROIs), analyzes their activity, decodes the activity into motor signals, and transmits them to the robot controller.

C. Encoding and Decoding Schemes

Encoding and decoding schemes are shown in Fig. 3. In the encoding part, a binary mechanism was chosen. To be specific, if the robot detects an obstacle, syringe pump B (connected to the inner pipette) pushes a small amount of glutamate solution to the Petri dish, while syringe pump A (connected to the outer pipette) constantly draws extracellular solution back, so as to confine the impact of glutamate in the sensory area. The syringe pump B holds if no obstacles are detected. Likewise, binary decoding

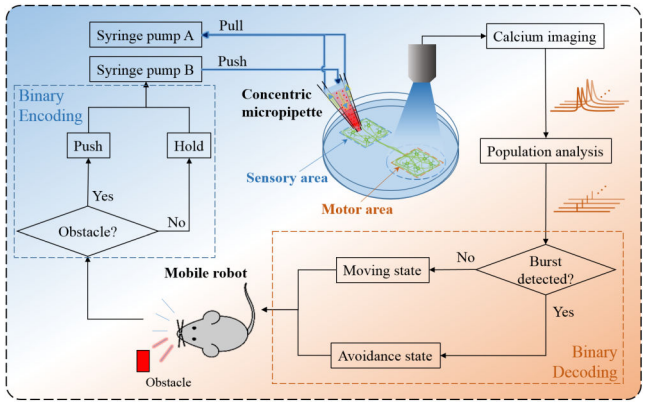

Fig. 3. Binary encoding (push or hold) and binary decoding (move or avoid) schemes for the proposed system.

was used. If an area-wide burst in the motor area is detected, that is, most of the neurons in the motor area fire a burst of APs simultaneously, the robot will enter an avoidance state to avoid collision with the obstacle, and then switches to a moving state for a certain period of time. Otherwise, the robot stays in the moving state.

III. Materials and Methods

A. Micro-Contact Printing

Petri dishes with modular cell-adhesive patterns were fabricated using micro-contact printing, which comprised two key processes: the fabrication of micro-stamps and the printing process for transferring protein patterns.

The micro-stamps were fabricated as follows. First, chrome plates with photoresist on soda-lime glass were purchased from Shaoguang Materials. Second, the chrome plate was cut into small square pieces of width 25 mm. Third, desired patterns were transferred to the chrome piece using direct laser writing using a Pattern Generator (microPG 101 from Heidelberg). Fourth, the exposed area was developed by AZ400 K (AZ Electronic Materials) 1:3 mixed with ultra-pure water ($> 18M\Omega*$cm, Purist UV from Rephile) for 7 min, and then etched by Chrome Etchant 18 (Dow Materials Science) for 1 min. Fifth, a polydimethylsiloxane (PDMS) stamp was fabricated by replica molding. PDMS pre-polymer (Sylgard 184 from Dow Corning) 10:1 mixed with curing agent was degassed at 5 °C for 30 min, and poured onto the chrome plate, followed by baking at 65 °C for 2 hours. Finally, the cured PDMS stamp was released from the chrome piece and cut into the desired shape. The fabricated PDMS stamps were stored in ultra-pure water when not used to increase the hydrophilicity.

The micro-stamps were used to transfer protein patterns as follows. First, the substrate of a 35 mm TC-treated Petri dish (Dow Corning) was pre-coated by 0.2% agarose (BioFroxx) solution (in ultra-pure water) to render the substrate cell-repellent. The agarose-coated Petri dish was then sterilized by ultraviolet radiation for an hour. Second, protein ink [0.1% ECM gel (E1270 from Sigma-Aldrich) + 50 μg/mL poly-D-lysine (PDL, P0899

from Sigma-Aldrich) in PBS buffer solution (Thermo Fisher Scientific)] (called PECM) was prepared. Third, the inking process. The modified stamp was put inverted on a clean Petri dish. 200 μL PECM solution was pipetted onto the surface to cover the raised pattern area for 5 min. Then, the stamp was taken out and dried by nitrogen quickly to avoid the formation of salt crystallization. Finally, the stamp was once again inverted and pressed against the agarose-coated Petri dish, with raised pattern against the substrate. A pressure of 300 g was applied for 2 min. After that, the stamp was released and the agarose-coated PECM-patterned substrate was obtained, which was sealed and stored in a sterile clean bench before use. A total of four Petri dishes were prepared, with each one containing 15 modular PECM patterns.

B. Culture of Neuronal Cells

Primary cortical neurons (OriCell SCCFN-00001, Cyagen Biosciences) from embryonic 18-day-old Sprague-Dawley rats were dissociated, cryopreserved in the preservation medium, transported on dry ice, and preserved in liquid nitrogen before use.

Right before plating, the cryopreserved primary neurons (2 million in a cryogenic vial) in 1 mL preservation medium were quickly thawed and mixed with 4 mL pre-warmed neuronal plating medium (MEM + 5% fetal bovine serum + 5% horse serum + 0.6% D-glucose). Then, neurons were plated at a density of 600 cells mm^{-2} on agarose-modified PECM-patterned substrates. After 4 hours, 2/3 medium was changed by neuronal culture medium (Neurobasal medium (Gibco) + 2% B27 + 1% GlutaMAX). One-third of the medium was changed every 4 days since day 4 with neuronal culture medium.

C. Calcium Imaging

All calcium imaging experiments were performed between 14 and 22 days in culture. In calcium imaging experiments, cultures were loaded with 4 μM calcium indicator Fluo-4/AM (Solarbio) and 0.01% Pluronic F-127 (Solarbio) in Mg $^{2+}$-free buffered saline solution (BSS, containing 130 mM NaCl, 5.4 mM KCl, 5.5 mM Glucose, 20 mM HEPES, and 1.8 mM $CaCl_2$ with the pH titrated to 7.4) at 37 °C for 40 min, rinsed by BSS, and incubated in BSS for another 10 min before observation. The calcium indicator-loaded cultures were then observed on an inverted microscope (IX73, Olympus) equipped with a 10x objective lens, a short-arc lamp (X-Cite 120Q, Lumen Dynamics), and a charge-coupled device camera (DP21, Olympus). All calcium imaging videos were recorded and presented in real-time by cellSens software at room temperature, with a temporal resolution of 80 ms (12.5 frames/s) and spatial resolution of 1200 $\times$ 800 pixel^2. The faintest level of excitation fluorescence was selected to reduce the adverse effects of photo-bleaching and photo-toxicity.

D. Global Chemical Modulation

Mg $^{2+}$-contained BSS (containing 120 mM NaCl, 5.4 mM KCl, 5 mM $MgCl_2$, 5.5 mM Glucose, 20 mM HEPES, and 1.8 mM $CaCl_2$ with the pH titrated to 7.4) was applied incrementally (20 μL per step) into the Mg $^{2+}$-free BSS (1 mL) to suppress the spontaneous network bursts. For different mBNNs, different concentrations of Mg^{2+} were required to make spontaneous bursts disappear, ranging from 283 μM to 536 μM.

E. Local Chemical Stimulation

200 μM glutamate (from Solarbio) solved in Mg $^{2+}$-free BSS was loaded in the inner pipette for local chemical stimulation. For the outer pipette, Mg^{2+}-free BSS was used. The coaxial needle (inner G25, and outer G18) was purchased from HZ Electrospinning. The two pipettes were pulled from a glass capillary by a glass puller (PC-10, Narishige). Two syringes connected to the inner and outer pipette through flexible tubes were fixed on two syringe pumps (Legato 100 and 111, KD Scientific). Pump A (connected to the outer pipette) and pump B (connected to the inner pipette) were preset to pull at 197.92 μL/h, and push at 42.46 μL/h, respectively. The pumps were controlled by the GUI automatically through serial ports. A 3-DOF micromanipulator (LDV50-LM-C2, Xinxingli Pneumatic) was used to hold the concentric pipette through three connecting pieces (custom-made from Wenext) and move it to desired positions.

F. Robot Simulation

The mobile robot was designed in the robot simulator CoppeliaSim, which consisted of a ball body, two independent active front wheels (for free moving and turning), one passive rear wheel (for support), and a proximity sensor (for obstacle detection). The proximity sensor sends a boolean 1 if it detects any obstacle in its sensory field, and sends a boolean 0 otherwise. A remote API was introduced to relay information between the simulator CoppeliaSim and the GUI (in the Matlab environment).

G. Robot Control Algorithm

To achieve the obstacle avoidance task, the robot has two motion states: moving and avoidance states. The neural activity in the motor area of the mBNN was recorded in real-time to determine whether the robot should switch from the moving state to the avoidance state. In the moving state, the left and right wheels move forward both at a speed of $3\pi/7$ rd/s; in the avoidance state, the left and right wheels rotate at speeds of $-\pi$ rad/s and $-\pi/7$ rd/s, respectively. These parameters were optimized to let the interval between two consecutive detections of obstacles be about 10 to 20 seconds. Each time a network burst was detected in the motor area, the GUI sends a signal to the simulated robot to switch from the moving state to the avoidance state. The robot stays in the moving state otherwise. If the robot switches to the avoidance state, after a certain duration t_{avoid}, the robot automatically switches back to the moving state. The t_{avoid} obeys a normal distribution with a standard error of 0.2 and a mean value of 2.0 s.

TABLE I
NOMINAL PARAMETERS OF THE CONCENTRIC MICOPIPETTE

Diameter (mm)	Inner	Outer
Inner pipette (tip)	0.070	-
Outer pipette (tip)	0.265	-
Inner needle	0.26	0.51
Inner pipette (bulk)	0.58	0.78
Outer needle	0.90	1.26
Outer pipette (bulk)	1.36	1.60

IV. EXPERIMENTS AND DISCUSSION

In this section, we first describe the fabrication of the cost-effective concentric pipette, and ascertain the optimal parameters of local chemical stimulation. Then, we verify whether the concentric pipette can confine the chemical-affected area in the sensory area. After that, we examine the hypothesis that whether inter-modular signal transmission can be evoked by local chemical stimulation after whole-field suppression with elevated $[Mg^{2+}]$. Finally, we demonstrate that the proposed mBNN-based neuro-robotic system can realize the stable interconnection between the mBNN and the robot through an active obstacle avoidance experiment.

A. Fabrication and COMSOL Simulation of the Concentric Pipette

The concentric pipette was fabricated based on a commercially available coaxial needle, which was soldered by two standard needles (inner G25, and outer G18). In addition, it contains two glass micropipettes pulled by a glass puller (PC-10, Narishige), with the detailed parameters shown in Table I. In this work, we need to apply local chemical stimulation on the whole sensory area (200-by-200 μm square), so we set the desired tip diameter of the inner and outer micropipettes as 50–100 μm and 250–300 μm, respectively. The assembled concentric pipette is shown in Fig. 4(a). During assembly, the end of the inner micropipette was touched with a little melted paraffin, and rapidly inserted into the gap between needles. The inner micropipette would be fixed when the paraffin solidifies. Then, the outer micropipette was inserted and fixed with parafilm. The proposed concentric pipette features a simple fabrication process and cost-effectivity, costing less than 40 dollars in addition to the glass puller.

Then, we demonstrate that the concentric pipette can confine the chemical stimulation in a limited spatio-temporal range, as shown in Fig. 4(d). The tip-to-bottom distance was optimized to be 150 μm, the flow rate of the inner and outer pipette being 2.67 mm/s and 1 mm/s, respectively. With these parameters, as shown in Fig. 4(f), the concentric pipette can confine the streamline in the outer pipette, while the streamline of the single pipette flows away. Moreover, when the inner pipette is shut down, the residual chemical will be drawn back to the outer pipette. Therefore, it can not only confine the chemical stimulation to a small area but also reduced its impact duration. In addition, we have also examined whether the induced shear stress will damage the cultured neurons. With the former parameters, shear stress at the bottom (maximum 0.2 Pa) remains in the long-term

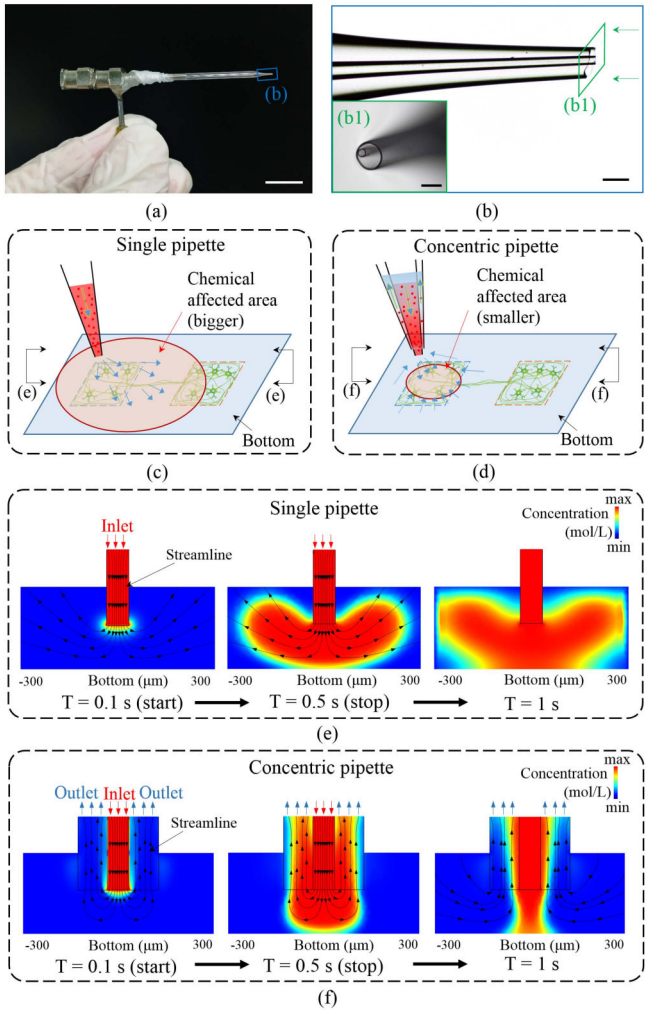

Fig. 4. Concentric micropipette and its comparison with single micropipette. (a) The assembled concentric micropipette. (b) Zoom-in view in (a). (c) and (d) are schematics of working principle of the single and concentric pipette. (e) and (f) are concentration fields and streamlines using the single and concentric pipette at different timepoints. Scale bar: 1 cm in (a) and 250 μm in (b).

($>$ a day, 0.025 Pa) and short-term safe range (for an hour, 0.038 Pa) [18], which paves the way for hour-long local chemical stimulation.

B. Verification of the Concentric Pipette

To verify the effectiveness of the concentric micropipette, we performed a local chemical stimulation experiment on some special mBNNs, where 1) the two areas of the mBNN are not connected by nerve bundles, 2) no network bursts were observed in Mg2+ free BSS, 3) sporadic and spontaneous sub-network bursts were observed on both areas. This happens to some of the mBNNs due to fabrication inefficiency (not enough PECM gels transferred in the connection area). In this experiment, only one area (the sensory area) of the mBNN is stimulated. Therefore, if the concentric micropipette cannot confine the chemical-affected zone to the stimulated area, the other area will also present induced bursts. As shown in Fig. 5, only bursts

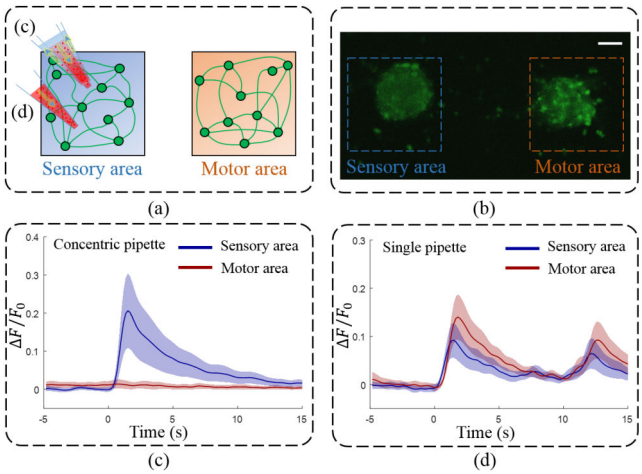

Fig. 5. Concentric micropipette can confine the chemical-affected zone to the sensory area. (a) Illustration of the verification experiment, in which neurons in the sensory and motor area are isolated from each other. (b) Epi-fluorescence view of the selected mBNN. Relative fluorescence traces of neurons in the motor and sensory area stimulated at 0 s by the concentric pipette (c) and by the single pipette (d) averaged across neurons (9 in sensory and 9 in motor) and trials (n=5 and n=3, respectively). Lines represent mean value, and the shadow represents standard deviation. Scale bar: 50 μm.

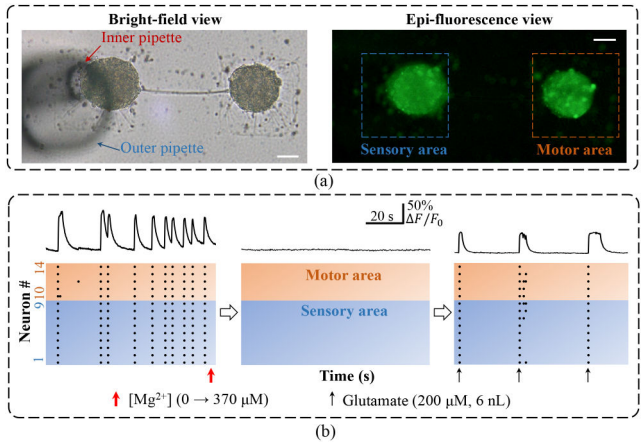

Fig. 6. Evoked inter-modular signal transmission in the mBNN. (a) Left: bright-field view of an mBNN with the concentric pipette positioned above its sensory area; right: the corresponding epi-fluorescence view. (b) Top panel: average relative fluorescence intensity of all neurons in motor area vs. time. Bottom panel: corresponding raster plot of neuronal bursts. Scale bar: 50 μm. .

in the nominal stimulation area (sensory area) were observed for the concentric group. However, when stimulated by the single pipette, both the neurons in the sensory area and in the motor area present sub-network bursts. We show that the concentric pipette has the advantage of confining the chemical (pharmacological)-affected zone to the sensory area of mBNN. This verification experiment was designed because we wanted to rule out the possibility that the bursts in the motor area are not induced by inter-modular signal transmission, but evoked by glutamate.

C. Inter-Modular Signal Transmission Evoked by Local Chemical Stimulation

After culture for 14 days, some mBNNs present spontaneous network-wide bursts. We choose these mBNNs as our subject of experiment for their innate ability of inter-modular signal transmission. The question becomes, how to suppress the spontaneous bursts while preserving the capability of the mBNN to transmit burst signals inter-modularly upon local chemical stimulation. To address this question, we tried to increase the extracellular $[Mg^{2+}]$, which reduces the current through NMDA receptors. Then, we exploited a kind of neurotransmitter (glutamate) as the chemical for local stimulation. After loading with calcium indicator Fluo-4/AM, the mBNNs were observed under an epi-fluorescence microscope, and a group of mBNN that can present spontaneous network-wide bursts was chosen. Then, the concentric micropipette was moved to the sensory area of the mBNN under the bright-field mode, with a top-to-bottom distance of 150 μm, as shown in Fig. 6(a). Next, the mBNN was observed under epi-fluorescence mode again. After recording the spontaneous neural activity for 100 s, 20 μL $[Mg^{2+}]$ solution (5 mM) was added to the 1 mL Magnesium-free buffer solution step-by-step. Local chemical stimulation starts after the spontaneous network-wide bursts disappear. During this process, the outer pipette constantly draws extracellular solution back, while the inner pipette pushes a small quantum of glutamate solution for 500 ms ($\sim$ 6 nL) at the specific time. A group of experimental results is shown in Fig. 6(b). At the bottom panel, each dot represents a neuronal burst, i.e., a burst of APs in a neuron. If in a short period of time (300 ms), most neurons ($>80\%$) in the sensory/motor area present neuronal bursts, then an area-wide burst is detected. If area-wide bursts in the two areas coincide in this period of time, it indicates inter-modular signal transmission appears. In Fig. 6(b), in the beginning, spontaneous network-wide bursts appear repeatedly (10 bursts in 2 min); when $[Mg^{2+}]$ is elevated incrementally, burst frequency decreases gradually (3, 1, 1 bursts in 2 min for 98, 192, 283 μM, respectively); when $[Mg^{2+}]$ is elevated to 370 μM (4 steps), no bursts are observed in 2 min; then, with local chemical (glutamate) stimulation of 6 nL, network-wide bursts reappear. Success rate of evoked inter-modular signal transmission are calculated as 89.2% (33 successes in 37 tests) at 0.05 Hz for 6 nL stimulation. For video version, see Supplementary Movie 1. These results demonstrate the feasible and reliable evoked inter-modular signal transmission by combing global chemical suppression and local chemical stimulation.

D. mBNN-Guided Active Obstacle Avoidance

Finally, we integrate the mBNN into our neuro-robotic system in a closed-loop to achieve the mBNN-guided robot active obstacle avoidance. As aforementioned, the system utilizes binary encoding and binary decoding schemes. Specifically, in the encoding part, if the robot detects obstacles, a certain amount of chemicals will be applied to the sensory area of the mBNN. In decoding, if the motor area presents an area-wide burst, the robot changes to an avoidance state and then switches back to the moving state after a certain time, which obeys a Gaussian

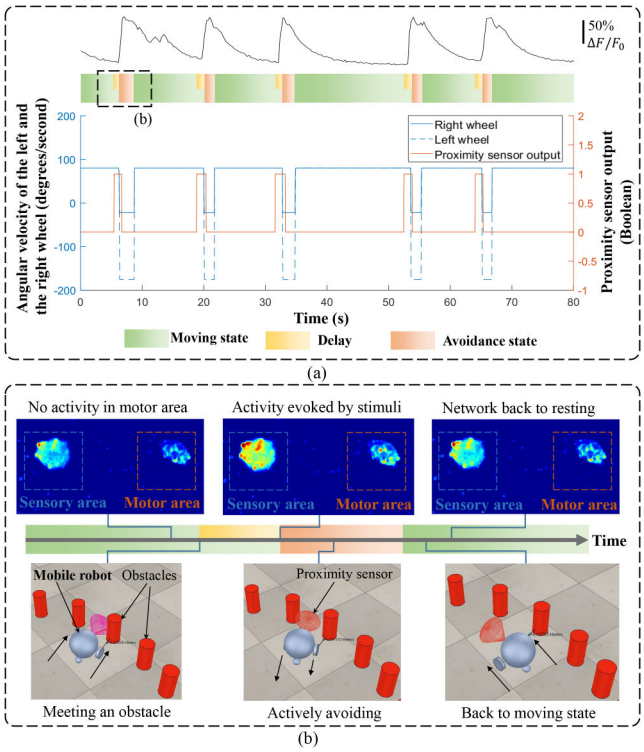

Fig. 7. Active obstacle avoidance guided by the mBNN. (a) Top panel: average relative fluorescence intensity of all neurons in motor area vs. time; bottom panel: corresponding running parameters of the robot. (b) How the mobile robot is guided by the mBNN to actively avoid obstacles. Top panel: false-color micrographs of the mBNN; middle panel: time axis; bottom panel: the mobile robot in different motion states.

distribution. The robot stays in the moving state otherwise. For specific parameters and optimization processes, see [19].

It should be mentioned that evoked inter-modular signal transmission, even with a high success rate (over 89% at 0.05 Hz for 6 nL stimulation), is possible to fail. In addition, refractoriness should be considered because stimulation less than 3 s after the last network-wide burst can hardly induce another network-wide burst. To avoid collision in these cases, the duration of local chemical stimulation is elongated (therefore neurotransmitter quantum increased) to the end of obstacle detection, and the robot is set to move at a low speed to avoid frequent obstacle detection. Experimental results are shown in Fig. 7. For video version, see Supplementary Movie 2. The delay, which is the time difference between the onset of obstacle detection and the turning of the robot is typically less than 1.2 s, with a mean of 830 ms, comparable to the reaction time of human brain.

E. Discussion

Research has shown that signal transmission between single neurons is unreliable, i.e., signals from pre-synaptic neurons cannot reliably induce observable signals in the post-synaptic neurons [11]. Interestingly, when many neurons wire together and form neural networks, signal transmission reliability is greatly enhanced [20]. However, when neurons form modular BNNs, the success rate of signal transmission across modules relies deeply on the connectivity between them [17]. Therefore, to realize reliable inter-modular signal transmission, we fabricated modular BNNs with strong inter-modular connectivity by micro-contact printing and high-density seeding. Spontaneous inter-modular signal transmission (network-wide burst) was observed in them [19]. However, these spontaneous signals will not only be mistakenly recognized as valid signals (false-positive mapping), but also may interfere with the transmission of valid signals due to refractoriness, so they need to be suppressed. But the suppression would inevitably reduce the inter-modular connectivity. Therefore, it's necessary to investigate whether such a range exists where spontaneous bursts disappear while the inter-modular signal transmission ability is preserved.

The NMDA receptors possess a Magnesium-dependence at low membrane potential, i.e., $[Mg^{2+}]$ blocks its ionic channels and reduces their EPSC [21]. Therefore, it can be utilized to reduce the network excitability, and inhibit the spontaneous network-wide bursts of mBNNs. We hypothesize that mBNNs suppressed by $[Mg^{2+}]$ still hold the ability of inter-modular signal transmission under local chemical stimulation. To verify this hypothesis, we examined mBNNs combining global chemical modulation (for suppressing spontaneous bursts) and local chemical stimulation (for inducing the evoked signal transmission). In order for the excitability of mBNNs to enter such a range, we elevated $[Mg^{2+}]$ incrementally and found out the concentration of just suppressing spontaneous bursts ranging from 283 μM to 536 μM, which varies for different mBNN (n = 4). These results are consistent with former research [16].

Moreover, to apply local chemical stimulation, a concentric pipette was fabricated. We verified that the proposed concentric pipette can confine the chemical-affected area in the sensory area, which paved the way for evoking trans-modular signal transmission using local chemical stimulation. Compared with existing research [20], [22], our concentric pipette features simple assembly and cost-effectiveness (less than \$40). Coupled with commercially available micromanipulators and custom-made connecting rods, local chemical stimulation can be achieved, costing less than \$200 in addition to syringe pumps. We believe this could reduce the barrier for practitioners from other areas (robotics in particular) to perform neuroscience experiments. In addition, this concentric pipette holds the potential of low delay, high temporal resolution, and scalability.

Finally, based on the mBNN capable of evoked inter-modular signal transmission, we engineered an mBNN-based neuro-robotic system. Compared with existing research, with most of them based on MEAs, the proposed system the proposed system can reach a high sensory-motor mapping success rate (89% in this work compared with 44.9% in [5] and 80% in [8]) via partial inhibition of NMDAR and local pharmacological stimulation.

In this work, we find calcium imaging with Fluo-4/AM suits our needs for the following reasons. First of all, calcium imaging enables easy and optical examination of bursts signals (accompanied by calcium elevation) of the mBNNs, which is suitable for us to examine the focus of this work: "whether such a range exists where spontaneous bursts in the mBNN are suppressed while the inter-modular signal transmission can still be evoked by local chemical stimulation. Second, the use of Fluo-4/AM as calcium indicator allows for at least 40 min continuous calcium recording

when using the faintest level of excitation fluorescence, which is enough since all the calcium imaging experiments in this work can be done in 30 min. Finally, the combination of micro-contact printing and calcium imaging presents us with many mBNNs for investigation, which compensates for the shortcomings of only short-term neural recording. Therefore, not only the difficulty of neural recording is largely reduced with the help of calcium recording, but many mBNNs can be prepared for investigation at the same time.

However, there are still challenges to be addressed for this neuro-robotic system to better capture biological intelligence. In nature, an organism's intelligence arises based on its ability to sense and adapt to the outer world. From this perspective, though the neuro-robotic system shows reliable sensory-motor signal transmission, which belongs to the reliable sensation to the outer world, it remains to be improved in reproducing intelligence of BNNs in vitro for the following reasons. First, the mBNN in the system can only receive binary signals with second-level intervals using chemical stimulation. Both the channel capacity and temporal resolution of information transmission are limited compared with living organisms and other MEA-based neuro-robotic systems [3], [4], [10]. Second, calcium recording can only detect bursts signals in sub-second level, which convey limited information regarding network plasticity and adaptive variation. Moreover, calcium imaging inhibits long term observation of plastic variations within the BNN due to photo-bleaching and photo-toxicity. To address these issues, MEA could be incorporated into the system, which enables higher channel capacity and temporal resolution using electrical stimulation, endowing the neuro-robotic system with rich sensation ability. In addition, MEA allows for sub-millisecond level monitoring of network plasticity as long as several months, suitable for long-term capturing adaption of BNNs [23]. Therefore, neuro-robotic systems combining multi-modal local and global stimulation (chemical and electrical) and recording (optical and electrical) techniques are promising in reproducing biological intelligence using mBNN.

V. Conclusion

In conclusion, this letter is characterized by a modular BNN (mBNN)-based neuro-robotic system with reliable inter-modular signal transmission (sensory-motor mapping) via local chemical stimulation and calcium imaging in closed-loop and in real-time. In this system, not only reliable evoked sensory-motor mapping in the mBNN is demonstrated, but it's also interconnected with a mobile robot to indicate whether an obstacle is met in front of it, and therefore whether the robot should steer clear of the obstacle or keep moving forward, hence achieving active obstacle avoidance. This system presents a novel platform to investigate how information is processed and transmitted in mBNNs, and also to examine the influence of local and global chemical modulation on within-network signal transmission. In the future, we intend to construct mBNNs with more complex modular structures in vitro and incorporate MEA into the system to train them to sense and adapt to the external world in long term, better reproducing the biological intelligence.

References

[1] T. B. Demarse, D. A. Wagenaar, A. W. Blau, and S. M. Potter, "The neurally controlled animat: Biological brains acting with simulated bodies," *Auton. Robots*, vol. 11, no. 3, pp. 305–310, 2001.

[2] T. Isomura, K. Kotani, and Y. Jimbo, "Cultured cortical neurons can perform blind source separation according to the free-energy principle," *PLoS Comput. Biol.*, vol. 11, no. 12, 2015, Art. no. e1004643.

[3] Z. Chen et al., "An overview of in vitro biological neural networks for robot intelligence," *Cyborg Bionic Syst.*, vol. 4, 2023, Art. no. 0001.

[4] M. Bisio et al., "Closed-loop systems and in vitro neuronal cultures: Overview and applications," in *Vitro Neuronal Networks*, Berlin, Germany: Springer, 2019, pp. 351–387.

[5] K. Warwick et al., "Controlling a mobile robot with a biological brain," *Defence Sci. J.*, vol. 60, no. 1, pp. 5–14, 2010.

[6] A. Novellino, P. D'Angelo, L. Cozzi, M. Chiappalone, V. Sanguineti, and S. Martinoia, "Connecting neurons to a mobile robot: An in vitro bidirectional neural interface," *Comput. Intell. Neurosci.*, vol. 2007, 2007, Art. no. 12725.

[7] Y. Yada, S. Yasuda, and H. Takahashi, "Physical reservoir computing with FORCE learning in a living neuronal culture," *Appl. Phys. Lett.*, vol. 119, no. 17, 2021, Art. no. 173701.

[8] Y. Li, R. Sun, Y. Wang, H. Li, and X. Zheng, "A novel robot system integrating biological and mechanical intelligence based on dissociated neural network-controlled closed-loop environment," *PLoS One*, vol. 11, no. 11, 2016, Art. no. e0165600.

[9] S. N. Kudoh, M. Tokuda, A. Kiyohara, C. Hosokawa, T. Taguchi, and I. Hayashi, "Vitroid–the robot system with an interface between a living neuronal network and outer world," *Int. J. Mechatronics Manuf. Syst.*, vol. 4, no. 2, pp. 135–149, 2011.

[10] B. J. Kagan et al., "In vitro neurons learn and exhibit sentience when embodied in a simulated game-world," *Neuron*, vol. 110, no. 23, pp. 3952–3969, 2022.

[11] J. A. Movshon, "Reliability of neuronal responses," *Neuron*, vol. 27, no. 3, pp. 412–414, 2000.

[12] J. Tessadori, M. Bisio, S. Martinoia, and M. Chiappalone, "Modular neuronal assemblies embodied in a closed-loop environment: Toward future integration of brains and machines," *Front. Neural Circuits*, vol. 6, 2012, Art. no. 99.

[13] T. T. Kanagasabapathi, D. Ciliberti, S. Martinoia, W. J. Wadman, and M. M. Decré, "Dual-compartment neurofluidic system for electrophysiological measurements in physically segregated and functionally connected neuronal cell culture," *Front. Neuroengineering*, vol. 4, 2011, Art. no. 13.

[14] T. T. Kanagasabapathi et al., "Functional connectivity and dynamics of cortical–thalamic networks co-cultured in a dual compartment device," *J. Neural Eng.*, vol. 9, no. 3, 2012, Art. no. 036010.

[15] J. Barral, X.-J. Wang, and A. D. Reyes, "Propagation of temporal and rate signals in cultured multilayer networks," *Nature Commun.*, vol. 10, no. 1, pp. 1–14, 2019.

[16] X.-s. Wang and E. I. Gruenstein, "Mechanism of synchronized Ca^{2+} oscillations in cortical neurons," *Brain Res.*, vol. 767, no. 2, pp. 239–249, 1997.

[17] H. Yamamoto et al., "Impact of modular organization on dynamical richness in cortical networks," *Sci. Adv.*, vol. 4, no. 11, 2018, Art. no. eaau4914.

[18] H. S. Shin, H. J. Kim, S. J. Sim, and N. L. Jeon, "Shear stress effect on transfection of neurons cultured in microfluidic devices," *J. Nanoscience Nanotechnol.*, vol. 9, no. 12, pp. 7330–7335, 2009.

[19] Z. Chen et al., "A real-time neuro-robot system for robot state control," in *Proc. IEEE Int. Conf. Real-time Comput. Robot.*, 2022, pp. 124–129.

[20] O. Feinerman, A. Rotem, and E. Moses, "Reliable neuronal logic devices from patterned hippocampal cultures," *Nature Phys.*, vol. 4, no. 12, pp. 967–973, 2008.

[21] R. A. Lester, J. D. Clements, G. L. Westbrook, and C. E. Jahr, "Channel kinetics determine the time course of NMDA receptor-mediated synaptic currents," *Nature*, vol. 346, no. 6284, pp. 565–567, 1990.

[22] O. Feinerman and E. Moses, "A picoliter 'fountain-pen' using co-axial dual pipettes," *J. Neurosci. Methods*, vol. 127, no. 1, pp. 75–84, 2003.

[23] D. A. Wagenaar, R. Madhavan, J. Pine, and S. M. Potter, "Controlling bursting in cortical cultures with closed-loop multi-electrode stimulation," *J. Neurosci.*, vol. 25, no. 3, pp. 680–688, 2005.